

# Towards enhancing the safety of Advanced Air Mobility: Automatic 3D inter-urban modelling for improved weather monitoring

Enrique Aldao Pensado<sup>1</sup>, Gonzalo Veiga Piñeiro<sup>1</sup>, Pablo Domínguez Estévez<sup>1</sup>, Fernando Veiga López<sup>1</sup>, Gabriel Fontenla Carrera<sup>1</sup>, Higinio González Jorge<sup>1</sup>, Elena Beatriz Martín Ortega<sup>1</sup>

<sup>1</sup> Research Institute of Physics and Aerospace Sciences, University of Vigo, Campus As Lagoas, Ourense, 32004, Galicia, Spain - (enrique.aldao.pensado, gonzalo.veiga, fernando.veiga, gabriel.fontenla, higinio, emortega)@uvigo.gal, pablo.dominguez.estevez@alumnado.uvigo.gal

**Keywords:** Automatic 3D geometry modelling, Data integration, Smart Cities, Advanced Air Mobility (AAM), Unmanned Aerial Vehicles (UAVs)

## Abstract

Advanced Air Mobility (AAM) is an emerging sector that aims to optimise transportation in urban and interurban environments using Unmanned Aerial Vehicles (UAVs). However, these aircraft are particularly susceptible to adverse weather phenomena, such as turbulence or wind gusts. To ensure the safety of operations, high-resolution real-time atmospheric prediction models, such as those based on Computational Fluid Dynamics (CFD), are required. The development of these systems faces challenges as accurate geometric models of navigation environments are needed to simulate the interaction between the wind and the terrain and infrastructure. These models feature complex geometries, so they cannot be manually crafted, requiring automated processing of geospatial data sources. As the main novelty, this work presents a methodology for the automated modelling of interurban environments for CFD simulations using digital elevation models and georeferenced surface semantic classification data. A practical case study was developed in the outskirts of Vigo (Spain), where we demonstrate the effectiveness of our approach and its integration with the open-source CFD software OpenFOAM.

## 1. Introduction

Advanced Air Mobility (AAM) is an emerging sector in the transportation industry that aims to introduce the use of Unmanned Aerial Vehicles (UAVs) for transporting people and goods in urban and interurban areas (Johnson and Silva, 2022), (Cohen et al., 2021). This will improve efficiency and reduce the costs of transportation by enabling the establishment of routes that minimise travel times and energy consumption. Additionally, AAM promotes the use of electrically powered aircraft and sustainable fuels, which will help reduce carbon footprint and provide a more accessible and eco-friendly mobility alternative (Al-Rubaye et al., 2023), (Bauranov and Rakas, 2021).

Despite the notable benefits for society, the implementation of these services requires the development of new technologies, infrastructures, and air traffic management systems to guarantee the safety of operations in the event of any incident (Takacs and Haidegger, 2022), (Reiche et al., 2021). One risk factor is the impact of atmospheric phenomena such as turbulence and wind gusts on UAV flight. These weather events arise from the interaction of the wind with the terrain and urban infrastructure, causing fluctuations in wind pressure and speed that can destabilise aircraft flight (Abbasi and Mahmood, 2019), (Oo et al., 2023), (Byrne et al., 2021). These phenomena pose a significant challenge since they can generate disruptions, delays, or even hinder the effective implementation of AAM (Steiner, 2019).

For these reasons, smart city models must incorporate systems for understanding and anticipating the formation of these weather events that can present scales on the order of a few metres. In this sense, high-resolution simulation techniques, such as Computational Fluid Dynamics (CFD) models, are required to resolve the intricacies of interurban flow patterns (Bender et

al., 2019). These systems simulate flow behaviour by discretising the Navier-Stokes equations within a finite volume computational domain and are capable of simulating phenomena on scales of several centimetres, thanks to Large-Eddy Simulation (LES) turbulence models (Tu et al., 2018). State-of-art works can predict wind patterns with average accuracies of around 0.25 m/s (Streichenberger et al., 2021).

Implementing these systems requires high-quality digital models of simulated areas, encompassing both geometry and surface properties. Acquiring these models is challenging as the complexity of interurban areas does not allow for manual modeling of geometries, requiring automated processing of geospatial information. Besides, most sources of georeferenced 3D information are oriented towards visualisation and animation applications (Google, 2023). Despite appearing visually consistent, these models may present errors such as absent surfaces, self-intersections, and non-manifold edges (Lee and Yang, 2019). Moreover, the spatial resolution of these sources is often excessively high and they do not provide information about the physical properties of terrain surfaces, complicating the processing and elaboration of the computational domain for CFD simulations.

As the main contribution of this study, we introduce a methodology for automatically generating meshes for CFD simulations of interurban environments, addressing the limitations for implementing these models. To achieve this goal, the system utilizes open-source digital terrain models along with semantic surface classification data to characterize terrain roughness and composition. In this way, CFD meshes are generated, compatible with the open-source software OpenFOAM, thus facilitating the development of intelligent urban atmospheric prediction models. To validate the results of our approach, a practical case study is conducted in the outskirts of the city of Vigo, Spain.

The remainder of this manuscript is organised as follows: Section 2 introduces the methodology of this article, covering the geometrical modelling of the case of study and the implementation of CFD simulations. In Section 3 the results are presented and analysed. Finally, Section 4 summarises the key findings of this paper and presents future works and improvements in this research line.

## 2. Methodology

As a practical case of study, a terrain situated on the outskirts of Vigo, Spain, was chosen (Figure 1). This area is of special interest, as it contains the main health centre of the city, which in the future could serve as a hub for the delivery of emergency medical supplies through UAVs. However, the zone features significant slopes and a high biodiversity, factors that contribute to the formation of turbulence and wind gusts, posing significant challenges to the safe flight of aircraft.

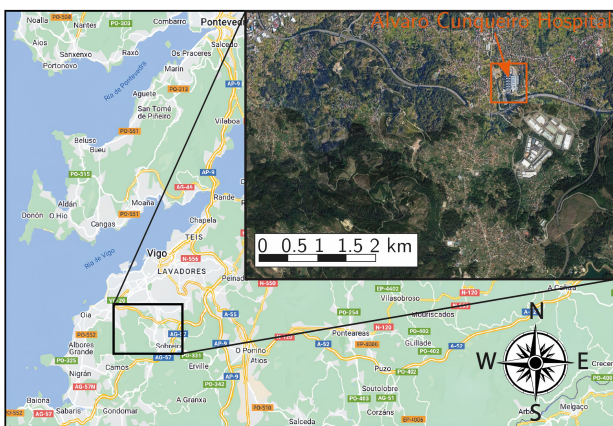


Figure 1. Area of study.

### 2.1 Terrain geometric modelling

To generate the environment model, firstly the 3D mesh of terrain was generated using a digital terrain model provided by the Spanish Geographic Institute (IGN) (IGN, 2023a). This product, represented in Figure 2, consists of a regularly spaced grid in UTM (Universal Transversal Mercator) coordinates that maps the terrain elevation with respect to sea level. These raster data were obtained from aerial LiDAR point clouds with an horizontal resolution of 25 metres and a height precision of 25 centimetres. As can be seen, the area features significant variations in elevation, ranging from 0 to 500 meters.

The 3D mesh of terrain was obtained by applying a Delaunay Triangulation to the points of the raster data, providing the 3D mesh depicted in Figure 3. This mesh exhibits significant slopes at the boundaries of the study case domain, which may lead to numerical instabilities in the CFD model. To address this issue, an entrance channel was added to the domain boundaries. This external surface consists of two parts, as shown in Figure 4.

1. *Constant Height Plane*: A flat surface with a constant height matching the median elevation at the terrain mesh boundaries. Its purpose is to facilitate organised inflow and outflow. It spans 250 meters, starting from the limits of the transition area.
2. *Transition Area*: This surface provides a smooth elevation transition between the terrain mesh and the constant height

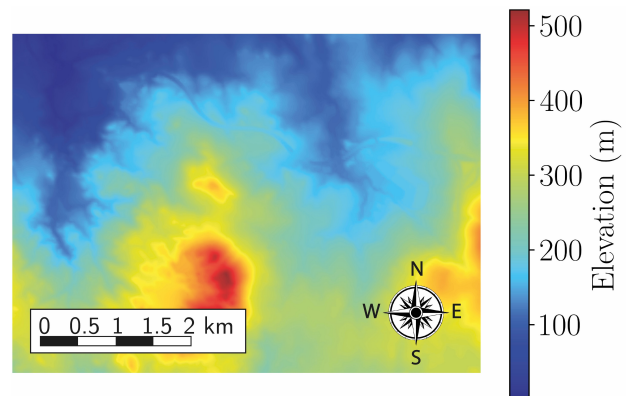


Figure 2. Digital Terrain Model of the area.

plane to prevent flow detachments. It spans 750 meters, in which the altitude varies linearly.

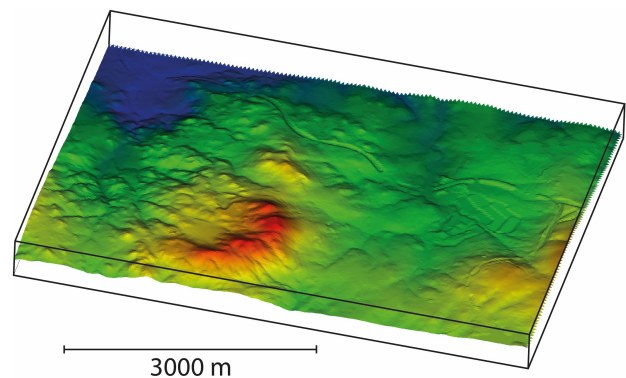


Figure 3. Terrain 3D mesh.

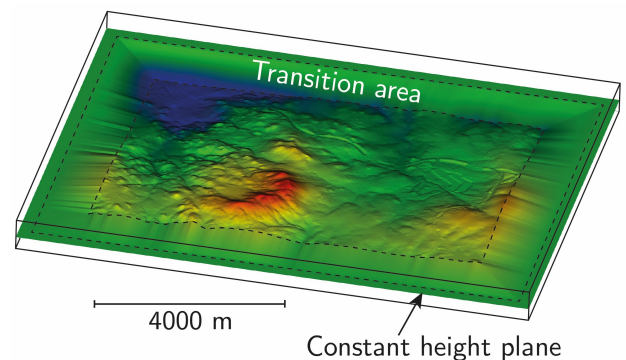


Figure 4. Final geometry including the entrance channel.

### 2.2 Terrain semantic classification

The surfaces of the 3D mesh depicted in Figure 4 were semantically classified to define the physical properties of terrain. For this purpose, the SIOSE AR model from IGN was used, a vector-format land use map that classifies the surfaces of the Spanish territory in different categories (IGN, 2023b). This product was created by combining various sources of information, including aerial LiDAR point clouds, aerial imagery, cadastral data, and declarations from farmers. To facilitate data processing, the map was transformed into a raster format with a resolution of 5 metres, as shown in Figure 5.

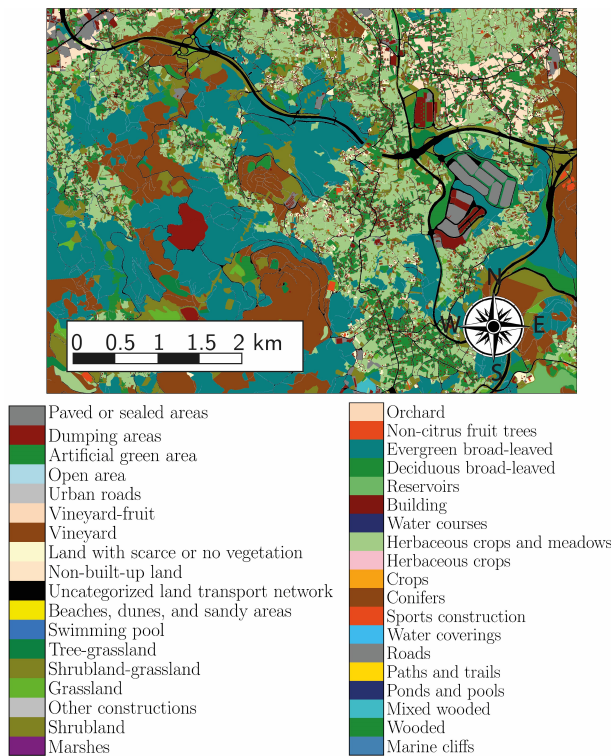


Figure 5. SIOSE AR Semantic Classification Model.

With this product, each triangle in the terrain mesh was assigned the corresponding category according to the position of its centroid. In this way, the geometry was semantically classified as shown in Figure 6. For the constant height plane and the transition zone, this semantic classification was not applied since they are artificially added elements only to improve the stability of CFD simulations.

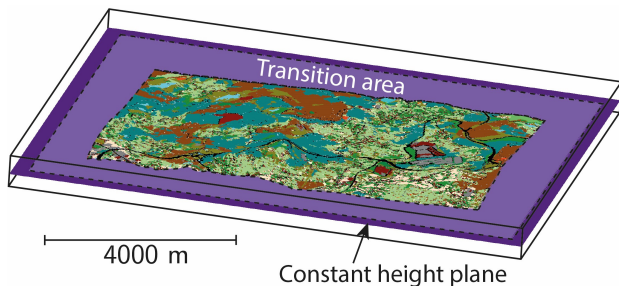


Figure 6. Semantically classified 3D mesh.

### 2.3 Computational domain mesh generation

The computational domain was generated using Ansys Workbench modelling software. Firstly, a rectangular parallelepiped was created covering the extended terrain mesh shown in Figure 6, with a height ranging from 0 to 1250 metres above sea level. Subsequently, a boolean operation was performed, removing the volume below the terrain surface, generating the computational domain shown in Figure 7.

Finally, the computational domain was meshed using a hybrid mesh composed of hexahedral, tetrahedral, and octahedral elements. This meshing method guarantees a robust and precise fit to the surface, with a high level of orthogonality and an aspect ratio close to one. In the areas near the terrain surface, local refinements were performed in order to reduce the values of  $y_+$

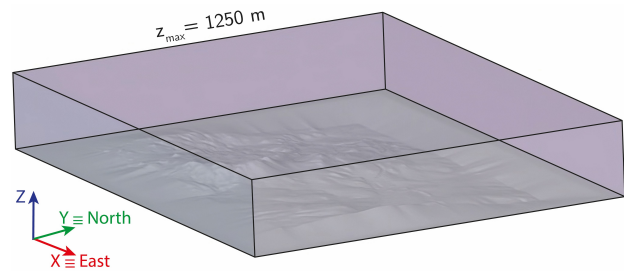


Figure 7. Computational domain.

and resolve the effects of boundary layer viscous dissipation. This process was carried out iteratively, checking the  $y_+$  results with the OpenFOAM utility checkMesh, until obtaining a suitable mesh for flow simulations. In this way, a high-resolution mesh consisting of 46.5 million cells was obtained.

It is important to note that the geometry of buildings and vegetation is not included in the terrain mesh due to memory and computational time limitations of CFD simulations. The current mesh covers several square kilometers and requires approximately 128 gigabytes of RAM and several hours of computation per simulation. The authors chose this approach because it concerns an interurban area with few buildings. The methodology presented in this work could be adapted to urban areas, including buildings, but it would be necessary to reduce the computational domain's extent to make it computationally feasible.

### 2.4 CFD simulation setup

SimpleFoam solver from OpenFOAM was employed for calculating the wind profiles. This is an open-source solver for incompressible and steady flows, widely employed for simulations in regimes of high Reynolds numbers. To replicate the effects of turbulent energy dissipation, the  $k - \epsilon$  turbulence model was used, which includes 2 additional equations to account for the effects of turbulence on the mean flow properties. One equation models the turbulent kinetic energy ( $k$ ) and the other the rate of dissipation of the turbulent kinetic energy, i.e.  $\epsilon$ . This RANS method was chosen due to its great balance between computational cost and precision in the scales of interest in this project. It should be noted that due to the complexity of the terrain's geometry and the scale of the computational domain, choosing a more detailed method is strongly discouraged due to the increase in computational cost that the change would produce in the problem.

To define the boundary conditions, Meteogalicia website was reviewed, the main meteorological agency in the region (Meteogalicia, 2023). According to the information provided by the agency, the predominant wind direction is 180 degrees, indicating south winds. For this reason, the south face of the computational domain was defined as the inlet, where Atmospheric Boundary Layer (ABL) conditions were imposed. The opposite face serves as the outlet, maintaining a constant pressure of 1 atmosphere. Symmetry conditions were applied to the lateral and upper faces, while in the ground surface, a wall model is applied employing a nutk wall function with variable roughness parameters. Figure 8 presents a scheme of the boundary conditions applied in this case of study.

For defining the roughness parameters of the nutk wall function, results from a previous work of Silva et al. were consulted (Silva et al., 2007). According to their findings, the roughness

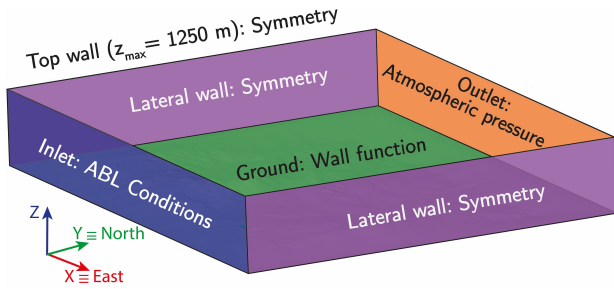


Figure 8. Boundary conditions.

values given in Table 1 were assigned to the different surfaces of the semantically classified 3D mesh.

Category	Roughness (m)
Mixed wooded, Wooded, Conifers, Tree-grassland, Evergreen broad-leaved, Deciduous broad-leaved	0.7
Crops, Herbaceous crops, Herbaceous crops and meadows, Orchard, Marshes, Shrubland, Grassland	0.1
Land with scarce or no vegetation, Open area, Non-built-up land, Reservoirs, Swimming pool, Water coverings, Beaches, dunes, and sandy areas, Ponds and pools, Dumping areas, Marine cliffs	0.05
Building, Sports construction, Other constructions	0.5
Paths and trails, Uncategorised land transport network, Urban roads, Paved or sealed areas	0.075
Transition area, Constant height plane	0.1

Table 1. Terrain roughness length values.

## 2.5 CFD data analysis

Finally, the CFD data were processed to provide a visualisation tool for assessing the impact of atmospheric turbulence on AAM operations. To characterise the turbulence intensity, the kinetic turbulence energy  $k$ , a quantity measuring the average kinetic energy of wind flow fluctuations, was employed. Thus, depending on the value of  $k$ , the flight conditions were classified as follows:

- *Safe flight* ( $k < k_{t1}$ ): Atmospheric turbulence poses no risk to the UAV.
- *Moderate turbulence* ( $k_{t1} < k < k_{t2}$ ): The UAV may experience certain turbulence conditions but remains safe for normal flight.
- *Hazardous flight* ( $k > k_{t2}$ ): Flight becomes dangerous due to severe turbulence conditions, and it is recommended to avoid aerial operations in these areas.

Where  $k_{t1}$  and  $k_{t2}$  are two threshold parameters adjusted based on the UAV characteristics.

## 3. Results

### 3.1 Wind simulations

Figures 9, 10 and 11 present the results of CFD simulations for different values of the input friction velocity  $v^*$ . This parameter represents the mean velocity at a characteristic height of the logarithmic profile of the ABL boundary conditions. High values of  $v^*$  represent atmospheric conditions with high wind intensity. The graphs show wind profiles at different height levels

above the ground (20, 40, 60, 80 m). As can be observed, the flow increases in velocity and becomes more uniform at higher altitudes above the ground, as the impact of terrain viscous dissipation decreases. Additionally, it can also be observed how in the furthest points of the terrain, the intensity of the wind increases, which could compromise the safety of operations, especially if aircraft are flying with crosswinds.

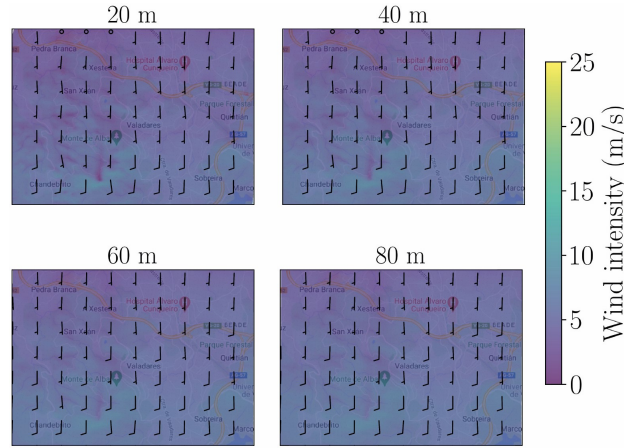


Figure 9. Wind profiles at different heights with respect to ground level. ( $u^* = 3$  m/s).

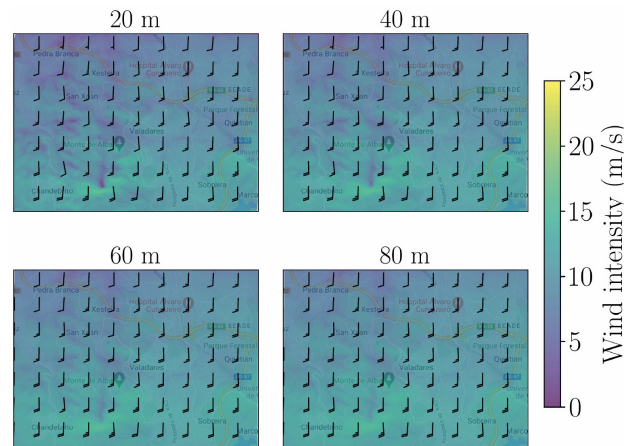


Figure 10. Wind profiles at different heights with respect to ground level. ( $u^* = 6$  m/s).

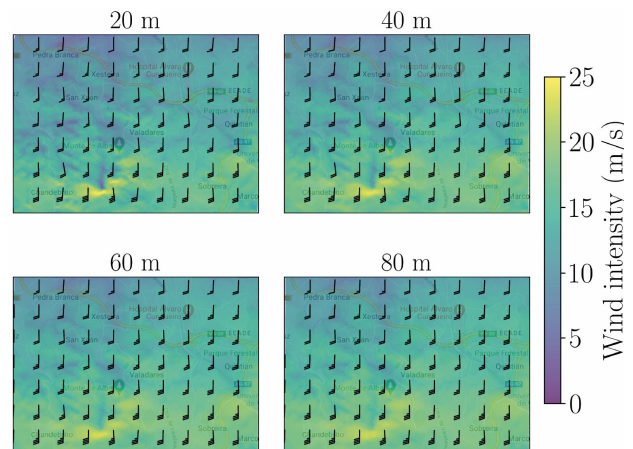


Figure 11. Wind profiles at different heights with respect to ground level. ( $u^* = 9$  m/s).

### 3.2 Turbulence assessment

Figures 12, 13, and 14 represent the kinetic turbulence energy  $k$  for different values of  $u^*$ . High inlet velocities increase the flow energy and facilitate the formation of zones with high turbulence intensity. As can be observed, in all the study cases, a flow instability region forms south of the computational domain near Monte de Alba.

This is due to the topography of the area, where mountains and significant terrain variations cause flow detachments and the development of turbulence. The most critical case is with  $u^* = 9$  m/s, where kinetic turbulence energies of up to 15 J/kg are reached.

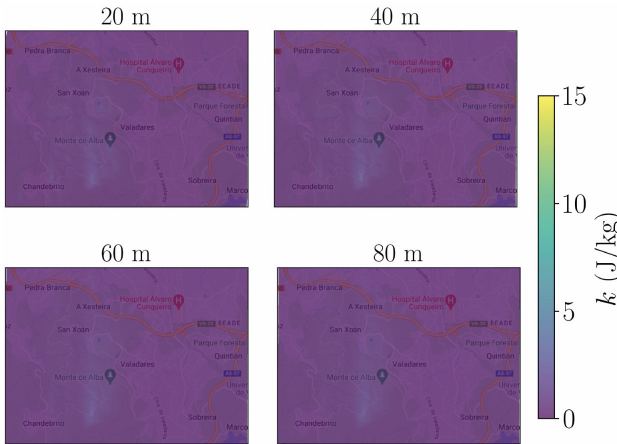


Figure 12. Kinetic turbulence energy results at different heights above terrain. ( $u^* = 3$  m/s)

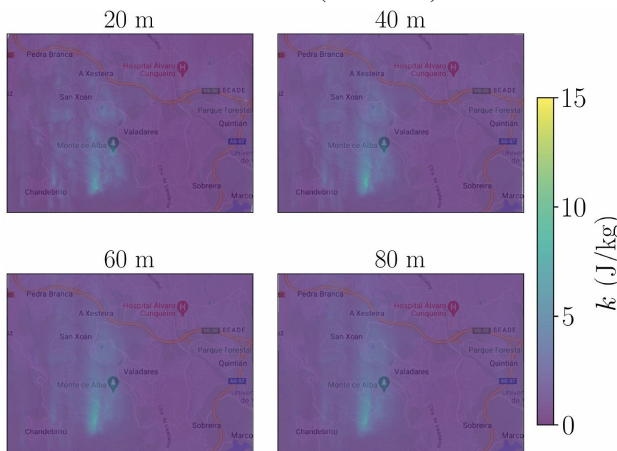


Figure 13. Kinetic turbulence energy results at different heights above terrain. ( $u^* = 6$  m/s)

Figures 15, 16, and 17 depict the airspace risk categorisation based on turbulent kinetic energy values. These risk maps were calculated considering parameters  $k_{t1} = 3$  J/kg and  $k_{t2} = 5$  J/kg, which in a real scenario would be set by the aircraft operator depending on the UAV's characteristics and the level of risk they are willing to assume. With the chosen configuration, for  $u^* = 9$  m/s, almost the entire airspace is considered dangerous for UAV operations, limiting the aircraft's operations in the area. For lower  $u^*$  values, the risk decreases due to the lower convective energy of the flow, with  $u^* = 3$  m/s being the safest, categorising the entire airspace as secure.

As can be seen in the results, if the friction velocity ( $u^*$ ) is high, practically the entire flight domain is categorized as unsafe due to the strong turbulence created in mountainous areas.

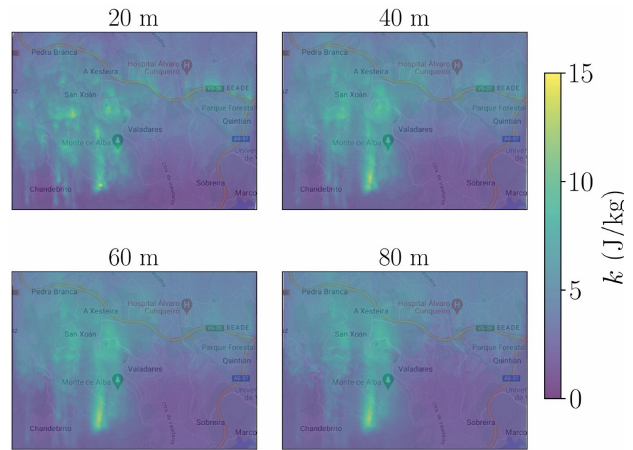


Figure 14. Kinetic turbulence energy results at different heights above terrain. ( $u^* = 9$  m/s)

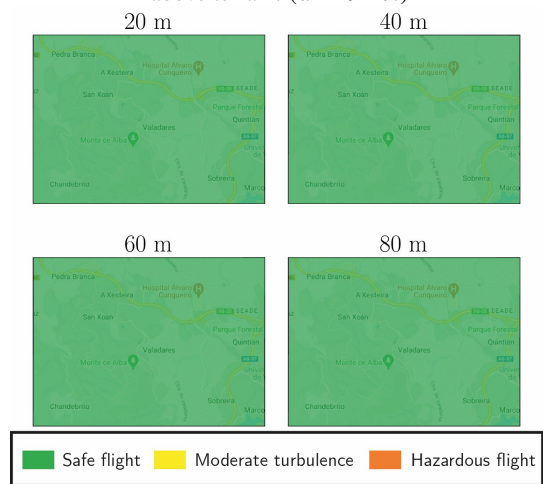


Figure 15. Airspace risk map categorisation ( $u^* = 3$  m/s).

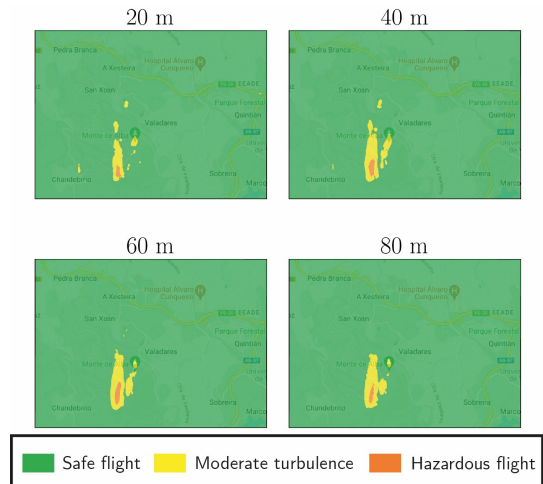


Figure 16. Airspace risk map categorisation ( $u^* = 6$  m/s).

This could hinder AAM (Advanced Air Mobility) operations, especially those of aircraft more susceptible to changes in wind speed. In light of these findings, the availability of these services could be compromised in the area during days of high wind intensity.

It is important to note that the terrain mesh does not include the geometry of buildings and structures due to the computational limitations of CFD, and the low building density of the area.

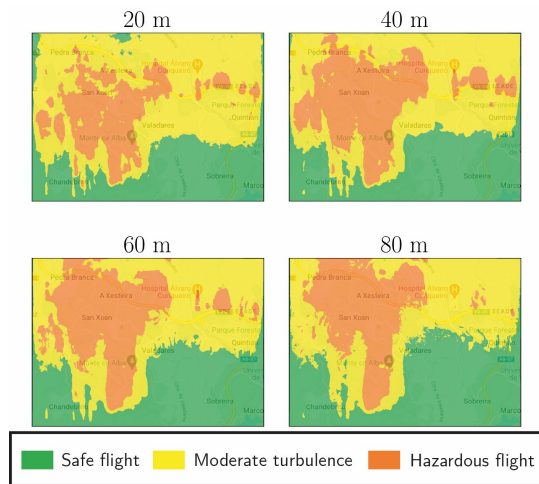


Figure 17. Airspace risk map categorisation ( $u^* = 9$  m/s).

However, if there were large constructions, this could cause considerable disturbances in the wind flow, further compromising AAM operations.

#### 4. Conclusions

This work presents a geospatial modelling methodology for the development of interurban microweather systems based on Computational Fluid Dynamics. Using open-source topography models and semantic terrain classification, a digital model of the environment was created by classifying surface roughness properties. From this geometry, a finite volume mesh compatible with OpenFOAM was developed, and several simulations were carried out under various wind conditions. Using simulation data, wind flow trends were analysed, and a methodology was implemented to characterise the operational risk based on turbulence kinetic energy values and two threshold parameters  $k_{t1}$  and  $k_{t2}$ .

The results indicated that in mountainous and uneven terrain, wind tends to create areas of high turbulence intensity, which poses a risk to UAVs. Especially, if the friction inlet velocity is high ( $u^*$ ), practically all areas of the computational domain exhibit strong fluctuations in wind velocity due to flow detachments created in mountainous areas. This could compromise aircraft safety and even hinder AAM operations.

In future work, the methodology of this study will be adapted for CFD simulation in urban areas. A trade-off will be conducted between the level of detail and the extent of the computational domain to ensure the viability of the simulations. Besides, the response of different commercial aircraft models to wind gusts will be analysed to adjust the risk thresholds  $k_{t1}$  and  $k_{t2}$ . Simulations will be conducted using dynamic UAV models and turbulence models calibrated based on CFD simulations. This approach will quantitatively characterise the risk of operations, thereby enhancing the understanding of the impact of turbulence on AAM operations.

#### Acknowledgements

Authors would like to acknowledge the funding from Agencia Estatal de Investigación and the European Union - NextGenerationEU, under grant numbers TED2021-129757B-C3 and PID2021-250600B-100. We also extend our appreciation to Xunta de Galicia for their funding support through the Galician

Marine Sciences Program under the Complementary R&D Plan. Additionally, we would like to thank Ministerio de Universidades as they support Enrique Aldao's PhD thesis through grant FPU21/01176.

#### References

- Abbasi, S. H., Mahmood, A., 2019. Bio-inspired gust mitigation system for a flapping wing UAV: modeling and simulation. *Journal of the Brazilian Society of Mechanical Sciences and Engineering*, 41, 524.
- Al-Rubaye, S., Tsourdos, A., Namuduri, K., 2023. Advanced Air Mobility Operation and Infrastructure for Sustainable Connected eVTOL Vehicle. *Drones*, 7(5).
- Bauranov, A., Rakas, J., 2021. Designing airspace for urban air mobility: A review of concepts and approaches. *Progress in Aerospace Sciences*, 125, 100726.
- Bender, A., Freitas, E. D., Machado, L. A. T., 2019. The impact of future urban scenarios on a severe weather case in the metropolitan area of São Paulo. *Climatic Change*, 156, 471-488.
- Byrne, R., Hewitt, N., Griffiths, P., MacArtain, P., 2021. Measured wind and morphological characteristics of a peri-urban environment and their impact on the performance of an operational large-scale wind turbine. *Journal of Wind Engineering and Industrial Aerodynamics*, 212, 104592.
- Cohen, A. P., Shaheen, S. A., Farrar, E. M., 2021. Urban Air Mobility: History, Ecosystem, Market Potential, and Challenges. *IEEE Transactions on Intelligent Transportation Systems*, 22(9), 6074-6087.
- Google, 2023. Google Earth. <https://earth.google.com/web/> (Last Accessed - 26th December 2023). Online.
- IGN, 2023a. Centro de Descargas (CNIG). <http://centrodedescargas.cnig.es/CentroDescargas/catalogo.do?Serie=LIDAR> (Last Accessed - 26th December 2023). Online.
- IGN, 2023b. SIOSE alta resolución. <https://www.siose.es/web/guest/siose-alta-resolucion> (Last Accessed - 26th December 2023). Online.
- Johnson, W., Silva, C., 2022. NASA concept vehicles and the engineering of Advanced Air Mobility aircraft. *The Aeronautical Journal*, 126(1295), 59-91.
- Lee, J., Yang, B., 2019. Developing an optimized texture mapping for photorealistic 3D buildings. *Transactions in GIS*, 23, 1-21.
- Meteogalicia, 2023. Histórico de la red meteorológica. <https://www.meteogalicia.gal/observacion/inicio.action> (Last Accessed - 26th December 2023). Online.
- Oo, N. L., Zhao, D., Sellier, M., Liu, X., 2023. Experimental investigation on turbulence effects on unsteady aerodynamics performances of two horizontally placed small-size UAV rotors. *Aerospace Science and Technology*, 141, 108535.
- Reiche, C., Cohen, A. P., Fernando, C., 2021. An Initial Assessment of the Potential Weather Barriers of Urban Air Mobility. *IEEE Transactions on Intelligent Transportation Systems*, 22(9), 6018-6027.

Silva, J., Ribeiro, C., Guedes, R., Rua, M.-C., Ulrich, F., 2007. Roughness length classification of Corine Land Cover classes. *Proceedings of EWEC 2007*.

Steiner, M., 2019. Urban Air Mobility: Opportunities for the Weather Community. *Bulletin of the American Meteorological Society*, 100(11), 2131 - 2133.

Streichenberger, B., Chakir, R., Jouy, B., Waeytens, J., 2021. Simulation and Validation of CFD turbulent airflow at pedestrian level using 3D ultrasonic anemometer in the controlled urban area “Sense-City”. *Journal of Wind Engineering and Industrial Aerodynamics*, 219, 104801.

Takacs, A., Haidegger, T., 2022. Infrastructural Requirements and Regulatory Challenges of a Sustainable Urban Air Mobility Ecosystem. *Buildings*, 12(6).

Tu, J., Yeoh, G.-H., Liu, C., 2018. Chapter 3 - governing equations for cfd: Fundamentals. J. Tu, G.-H. Yeoh, C. Liu (eds), *Computational Fluid Dynamics (Third Edition)*, third edition edn, Butterworth-Heinemann, 65–124.